A Novel Stochastic Unscented Transform for Robust State Estimation Enabling Enhanced Space Domain Awareness

Gerardo Josue Rivera Santos
West Virginia University

Jacob D. Griesbach
ARKA/Stratagem

Rachit Bhatia, Piyush M. Mehta
West Virginia University

ABSTRACT

IARPA's SINTRA program challenge to detect and track lethal non-trackable (LNT) objects is crucial for mitigating collision risks and maintaining the safety of space. These objects are often too small to be tracked effectively using conventional methods, thus making them a threat to operational satellites or other resident space objects (RSOs). It is not only important to maintain custody but also to ensure that a realistic covariance is sustained, as covariance information is crucial for robust decision-making, and provides a more comprehensive understanding of the dynamic nature of space systems. This paper presents a mathematical formulation for a new stochastic unscented transform (SUT) to incorporate the additional statistics of probabilistic models. Because of its generic nature, this framework has a myriad of applications in various fields. The new stochastic unscented approach is particularly advantageous in complex environments where traditional deterministic models are insufficient and modeling using Monte Carlo techniques will be inefficient. The derivation and validation of the new SUT algorithm has been previously performed for the primary motivating example of accurately capturing the joint statistics of probabilistic inputs driving stochastic density models for drag modeling in low Earth orbit (LEO). Here, the SUT extends the prior work by proposing a generalized method to incorporate such probabilistic models for space object tracking and space domain awareness. In this work, the SUT has been embedded within the CAR-MHF (Constrained Admissible Region-Multi Hypothesis Filter) algorithm to enhance its ability to model atmospheric density for LEO drag force modeling. This enables more accurate modeling of the dynamics and, thus, allows one to reduce process noise for un-modeled force perturbations. The SUT's ability to handle stochastic dynamics provides a more realistic representation of the space environment, enabling CAR-MHF to make more informed multiple hypothesis decisions based on probabilistic predictions.

1. INTRODUCTION

Over the decades, there has been a proliferation of Resident Space Objects (RSOs) in Low Earth Orbit (LEO). The IARPA SINTRA[1] program challenges one to detect and track space objects that are currently undetectable or non-trackable with current space surveillance network (SSN) technology. This brings forth the need to enhance space domain awareness (SDA) and space traffic management (STM) to prevent RSOs and debris collisions. Therefore, it is critical to persistently track and maintain custody of all space objects. With this realization, space object uncertainty/covariance knowledge is as important as knowledge of the state vectors themselves. Uncertainty quantification has shown to improve and enhance realism in the orbital states [1]. Studies such as [2, 3] have recently demonstrated the integration of stochastic or probabilistic models for the uncertain parameters (drag coefficient, C_D and atmospheric density ρ) that feed orbital drag dynamic modeling in LEO.

[1]This research is based upon work supported in part by the Office of the Director of National Intelligence (ODNI), Intelligence Advanced Research Projects Activity (IARPA), via 2023-23060200005. The views and conclusions contained herein are those of the authors and should not be interpreted as necessarily representing the official policies, either expressed or implied, of ODNI, IARPA, or the U.S. Government. The U.S. Government is authorized to reproduce and distribute reprints for governmental purposes notwithstanding any copyright annotation therein.

The novel Stochastic Unscented Transform (SUT) framework [4], used here for the orbital propagation application, was motivated by the need to the estimate the joint statistics of atmospheric density output resulting from probabilistic driver/inputs (e.g. $F_{10.7}$ [5]) feeding into stochastic density models (e.g. CHAMP-ML [6]). This work stemmed from the natural follow-on question and desire to incorporate this new probabilistic density modeling into covariance propagation and orbit determination. So, this work builds upon a new probabilistic drag model that also employs SUT, folding its effects into a larger orbit propagation context.

Historically, operational dynamics models, such as those estimating atmospheric density, are either physics based or empirical. In the empirical case, models rely on satellite data, which include HASDM [7] and MSIS [8]. Physics based models, like TIE-GCM [1] and WAM-IPE [9], employ the use of equations representing physical processes. Limitations of the operational HASDM system include being deterministic and highly simplified treatment of uncertainty. Recently, new machine learning (ML) based probabilistic models have establish a new foundation of models that provide uncertainty estimates overcoming deterministic limitations or previous models. Such new models include HASDM-ML [10], MSIS-UQ [11], CHAMP-ML [6], and TIE-GCM ROPE [12]. The main characteristic of these new models is that they provide output uncertainty alongside their atmospheric density model estimates. In addition, as for TIE-GCM ROPE, reduced computational complexity is observed with the replacement of ML inference over the use of physics equations through an emulator.

The stochastic density models described above need space weather drivers such as $F_{10.7}$ and A_p as inputs. These drivers need to be forecasted for orbit prediction adding another layer of uncertainty to the drag model. Several efforts over the years have resulted in the development of probabilistic drivers. One such recent development [5] has shown robust uncertainty quantification while outperforming operational forecast performance for $F_{10.7}$. As a result, accurately characterizing the uncertainty in density estimates requires account for the uncertainty in driver/input and the uncertainty of the density model itself.

Monte Carlo (MC) is typically used to capture meaningful statistics from probabilistic models. However, the excessive number of samples needed for accurate estimation renders MC inefficient. Another method, the Unscented Transform (UT) [13], was derived to track Gaussian statistics using a set of smartly sampled data points called sigma points. These points are selected from the statistics of the input distribution and weighted accordingly. Further UT adoption rose due to limitations of the extended Kalman filtering (EKF) [14], where it linearizes dynamics with Jacobian matrices which are difficult to compute. UT extends to various approaches, such as Unscented Kalman Filtering [15] and Unscented Schmidt-Kalman Filter (USKF) [16]. In UKF, the UT is applied for covariance propagation, while USKF extends UKF by implementing additional consider parameters for measurement bias estimation.

Historically, UT and Kalman filtering techniques are commonly applied in orbit determination (OD) [17]. Generally, in OD, a sequence is followed. First, Initial orbit determination (IOD) [18] is done by estimating a new/initial state vector where sufficient (usually multiple) measurements are collected to cover a full 6-dimensional state space. Then, OD state updates are implemented with subsequent observation measurement data. The state updates produce measurement residuals which are optimally minimized with Kalman filtering. In certain scenarios, where IOD is hard to implement due to limitations of the data, a constrained admissible region (CAR) can be used allowing multiple candidate initial state hypotheses to be generated from a single angle/angle-rate observation. The nature of this approach creates a situation where multiple filters becomes a necessity. This is where a constrained admissible region multiple hypothesis filter (CAR-MHF) [19] is used, which provides IOD and state update without apriori state knowledge. This approach is favorable not only for OD but also for characterizing atmospheric drag states.

The standard dynamic methods for orbit propagation are typically deterministic. Because they return values without conveying model uncertainty, these values are used as the "truth", meaning the uncertainty is conveyed as zero. Generally, we need to use process noise to compensate for these dynamics and unknown "untruths". Some methods include state noise compensation (SNC) for cases like obtaining the process noise covariance at small eccentricities for orbital states [20] and dynamic model compensation (DMC) [21]. But because these methods involve trial-and-error approaches to quantify dynamic unknown-unknowns, this is not too appealing. The effect of adding noise can provide stability and prevent systems from being overconfident in the face of uncertain dynamics, but it lacks the ability to efficiently capture or understand the realistic factors that are occurring. To reduce this problem, we tend to optimize the noise to avoid divergence and inconsistencies [22]. The adjustments of this noise provides the benefit of enhancing realism, but it can be difficult and tedious.

For the first time, having probabilistic density models, provides us with the benefit of developing a new mathematical

framework that implements an efficient method accounting for input and model uncertainty effects. Mentioned earlier, the method is named Stochastic Unscented Transform (SUT). The approach captures an overall system covariance by propagating the sigma points through a probabilistic model. Conventionally, a (deterministic) unscented transform (UT) is limited to tracking a set of smartly sampled sigma points to approximate the input probability distribution. However, with SUT, the uncertainty associated with the underlying system model can also be incorporated. This allows more accurate modeling of systems that can estimate uncertainty and capture complex dynamics more realistically. This method will grant an ability to have a stochastic output relying less on process noise to enhance the realism in orbit determination and propagation analysis as it properly accounts for dynamic uncertainties. The approach offers an improvement in the techniques for space domain awareness (SDA) and space traffic management (STM), where some contributions done in the past are: reliance for precision tracking along with characterization and modeling of the environment [23] and improve collision avoidance analysis showing optimal timelines for risk mitigation using time of closest approach (TCA) [24]. This novel framework can enable a significant improvement in space tracking and catalog maintenance with reduced computational burden, thus leading to enhanced SDA.

The paper will be arranged in the following way: First the concepts of the deterministic UT will be shown to establish the baseline. Second we will display the theory behind the mathematical SUT framework and display the end derivations of the study. Third we will show results of using SUT with CAR-MHF where a LEO space object is processed using CAR-MHF to compare both the standard (deterministic) UT and the new SUT. Finally, we discuss conclusions and potential future work.

2. SUT METHODOLOGY

2.1 Problem Statement

The goal of SUT framework is to accurately model the statistical mean and variance for a system using a probabilistic model driven by probabilistic inputs. Any given system can be broadly segmented into three basic components: input, model, and output. Each of these components can be deterministic or probabilistic. While previous studies have investigated systems with probabilistic inputs/outputs, no generic framework exists for incorporating a probabilistic model without linearizing or incorporating some form of approximation.

In the SUT framework, sigma points are defined as a specific set of data points collected from the input distribution. The input can generally have any arbitrary distribution, however, in this work, we consider the input distribution as a best-fit Gaussian distribution. (Similar to a standard unscented transform, the modeling seeks to incorporate and track the first two distribution moments, whether the input distribution is Gaussian or not. Other works investigate capturing higher order moments for cases where it may be needed [25].) Each sigma point includes the effects of uncertainty applied on the input distribution, such that the mean and variance of each sigma point is transformed through the stochastic model to produce new/transformed mean and variance. For N sigma points:

$$\mu_{x_0}, \quad \mu_{x_1}, \quad \ldots, \quad \mu_{x_N} \longrightarrow \begin{Bmatrix} \mu_{y_0} \\ \sigma^2_{y_0} \end{Bmatrix}, \quad \begin{Bmatrix} \mu_{y_1} \\ \sigma^2_{y_1} \end{Bmatrix}, \quad \ldots, \quad \begin{Bmatrix} \mu_{y_N} \\ \sigma^2_{y_N} \end{Bmatrix}$$

where sigma points, $x_0, x_1, x_2, ..., x_N$, smartly sampled from an input distribution, X, are fed through the model to obtain the output points, $y_0, y_1, y_2, ..., y_N$, where each output point is conveyed as a mean and variance, as illustrated in Figure 1. The approach is to treat each sigma point output shown above as best-fit, normally-distributed random variables. Once the input distribution sigma points and weights are defined, these data points are transformed by a probabilistic model to compute output information statistics. These (multiple) sigma-point statistics are then used to compute the overall system transformation distribution, Y, not only incorporating the properties of the input distribution, but also the uncertainties associated with the model transform itself.

2.2 Standard "Deterministic" Unscented Transform

The common approach known for the Unscented Transform is to track the first and second moments of an input distribution through a (semi-) arbitrary nonlinear function [26]. We call this standard unscented technique "deterministic" because it treats the underlying transformation as a deterministic model; it does not consider any uncertainty from the model/transformation itself. Here, provided an input value, the model provides a (deterministic) output value with no reported uncertainty.

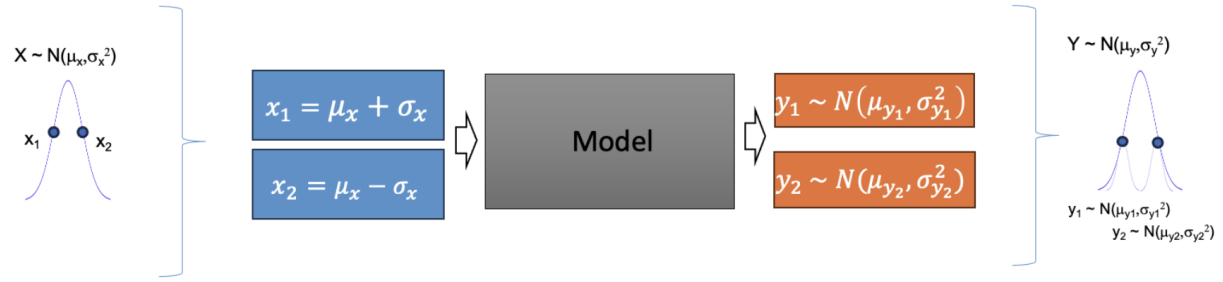

Fig. 1: Schematic Diagram of the SUT framework.

By choosing smartly sampled sigma points along with only attempting to track the first and second order moments, applying an unscented approach is more efficient than Monte Carlo or particle filtering techniques. The principle of this idea stands by selecting specific points known as *sigma points* obtained from the Gaussian input distribution's mean $\tilde{\mu}_x$ and variance $\tilde{\sigma}_x^2$. While the methodology within the paper can address higher-dimensional cases, we only address a single dimension (1D) herein. With this information, the sigma points and a set of weights can be obtained. The input sigma point values are defined as x_i with selected unscented weights for mean estimation, w_i^a, and variance, w_i^c, estimation. From previous contributions, different algorithms exist to select sigma point locations and weights using a set of scaling parameters [27].

Let the location of the sigma point relative to the mean (in units of standard deviations or σ) be defined as s_i, so that sigma-points are located at $\mu + s_i\sigma$. For example, $s_i = 1$ defines a sigma-point located at $\mu + 1\sigma$, and $s_i = -1$ defines a sigma-point located at $\mu - 1\sigma$. Then weights may be selected arbitrarily as long as they follow

$$\sum_{i=0}^{N} w_i^a s_i = 0 \tag{1}$$

$$\sum_{i=0}^{N} w_i^a = 1 \tag{2}$$

for the mean estimator, and for a valid variance estimator,

$$\sum_{i=0}^{N} w_i^c = 1 \tag{3}$$

$$\text{with } w_i^c = 0 \quad \text{for/if} \quad s_i = 0. \tag{4}$$

Adherence to the above constraints ensure that the sigma points can result in unbiased overall system estimates.

By translating the input sigma point values, x_i, through the (deterministic) model, f, we obtain output values as

$$y_i = f(x_i). \tag{5}$$

where we can estimate the desired statistics of the overall system mean μ_y and variance σ_y^2 as

$$\tilde{\mu}_y = \sum_{i=0}^{N} w_i^a y_i \tag{6}$$

$$\tilde{\sigma}_y^2 = \sum_{i=0}^{N} \frac{w_i^c}{s_i^2} (y_i - \tilde{\mu}_y)^2, \tag{7}$$

where we use a tilde to denote estimated values.

The above equations may be proven by inserting the input sigma points x_i into Equations (6) and (7) and the result would match the mean μ_x and the variance σ_x, respectively.

The investigations developed in this work led us to analyze a case of a common set of $N = 2$ sigma points chosen simply at $\mu \pm \sigma$.

2.2.1 Common Symmetric $N = 2$

Here, sigma points are selected by evenly weighting two data points around the mean. The collection of these points are $x_0 = \mu_x + \sigma_x$ and $x_1 = \mu_x - \sigma_x$. By the nature of the symmetric approach, when the average is taken for both sigma points, we obtain the mean of the input distribution. To preserve this observation, the value for the weights of each point are $w_0^a = w_1^a = w_0^c = w_1^c = \frac{1}{2}$. With this, the mean (6) and covariance (7) can be rewritten as

$$\tilde{\mu}_y = \frac{1}{2}(y_0 + y_1) \tag{8}$$

$$\tilde{\sigma}_y^2 = \frac{1}{4}(y_0 - y_1)^2 \tag{9}$$

We choose this (common symmetric $N = 2$ case) for its simplicity. Other cases may be considered such as asymmetric cases (where $w_i^a \neq w_i^c$) and also cases with additional sigma points.

2.3 Stochastic Unscented Transform

The next step is to evolve the unscented transform to incorporate probabilistic modeling (using the symmetric case). The main characteristic of this method is that we are implementing the same rules as the deterministic unscented transform, but instead of having scalars, we are working with model *output distributions*. Here, model outputs are provided as a mean value with an associated uncertainty variance, $y_i = (\mu_{y_i}, \sigma_{y_i}^2)$. Also, importantly, we assume herein that each resultant sigma point distribution is independent.

Considering the deterministic mean and variance estimators, we derive new stochastic mean and variance estimators by carrying through each sigma-point output result as a distribution. Here we denote Y as the overall system output distribution.

2.3.1 General Mean Estimator

Using (6), the resultant mean is the weighted sum of all of the y_i output sigma points. Based on this, we develop a general mean estimator that can be applied to any set of sigma points with their appropriate weights. Since each Y output sigma point represents a normal distribution, the distribution for the weighted sum associated with the mean estimator for Y can be described as

$$\sum_{i=0}^{N} w_i^a \mathcal{N}\left(\mu_{y_i}, \sigma_{y_i}^2\right) \sim \mathcal{N}\left(\sum_{i=0}^{N} w_i^a \mu_{y_i}, \sum_{i=0}^{N} (w_i^a)^2 \sigma_{y_i}^2\right) \sim \mathcal{N}\left(\tilde{\mu}_y, \tilde{\sigma}_{\mu_y}^2\right), \tag{10}$$

again assuming each sigma point is independently distributed. Thus,

$$\tilde{\mu}_y = \sum_{i=0}^{N} w_i^a \mu_{y_i} \tag{11}$$

$$\tilde{\sigma}_{\tilde{\mu}_y}^2 = \sum_{i=0}^{N} (w_i^a)^2 \sigma_{y_i}^2 \tag{12}$$

The weighted sum of (independent) normal distributions remains normal, where weighted means and squared weighted variances add. It is important to note that $\tilde{\sigma}_{\tilde{\mu}_y}^2$ is the estimated variance of the mean estimator, and not the Y system variance. $\tilde{\sigma}_{\tilde{\mu}_y}^2$ conveys the uncertainty of the mean estimator.

2.3.2 General Variance Estimator

For the variance estimator stemming from Equation (7), one can use the generalized χ^2 formulation in the appendix of [4] to compute a generalized variance estimator for any given UT weights and sigma points. Noting that the distribution of the mean estimator is given in Equation (10), one can derive the distribution of the variance estimator by substituting the sigma point distributions into (7) as[2]

$$\sum_{i=0}^{N} \frac{w_i^c}{s_i^2} \left(\mathcal{N}\left(\mu_{y_i}, \sigma_{y_i}^2\right) - \mathcal{N}\left(\tilde{\mu}_y, \tilde{\sigma}_{\tilde{\mu}_y}^2\right) \right)^2 \sim \sum_{i=0}^{N} \frac{w_i^c}{s_i^2} \left(\mathcal{N}\left(\mu_{y_i} - \tilde{\mu}_y, \sigma_{y_i}^2 + \tilde{\sigma}_{\tilde{\mu}_y}^2\right) \right)^2 \tag{13}$$

$$\sim \tilde{\chi}^2 \left(\begin{bmatrix} \frac{w_0^c}{s_0^2}\left(\sigma_{y_0}^2 + \tilde{\sigma}_{\tilde{\mu}_y}^2\right) \\ \frac{w_1^c}{s_1^2}\left(\sigma_{y_1}^2 + \tilde{\sigma}_{\tilde{\mu}_y}^2\right) \\ \vdots \\ \frac{w_N^c}{s_N^2}\left(\sigma_{y_N}^2 + \tilde{\sigma}_{\tilde{\mu}_y}^2\right) \end{bmatrix}, \begin{bmatrix} 1 \\ 1 \\ \vdots \\ 1 \end{bmatrix}, \begin{bmatrix} \frac{\left(\mu_{y_0} - \tilde{\mu}_y\right)^2}{\sigma_{y_0}^2 + \tilde{\sigma}_{\tilde{\mu}_y}^2} \\ \frac{\left(\mu_{y_1} - \tilde{\mu}_y\right)^2}{\sigma_{y_1}^2 + \tilde{\sigma}_{\tilde{\mu}_y}^2} \\ \vdots \\ \frac{\left(\mu_{y_N} - \tilde{\mu}_y\right)^2}{\sigma_{y_N}^2 + \tilde{\sigma}_{\tilde{\mu}_y}^2} \end{bmatrix} \right) \tag{14}$$

With this and the known equations for generalized χ^2 mean and variance (see appendix of [4]), the above generalized variance estimator distribution has mean and variance as

$$\tilde{\sigma}_y^2 = \sum_{i=0}^{N} \frac{w_i^c}{s_i^2} \left(\sigma_{y_i}^2 + \tilde{\sigma}_{\mu_y}^2 + (\mu_{y_i} - \tilde{\mu}_y)^2 \right) \tag{15}$$

$$\sigma_{\tilde{\sigma}_y^2}^2 = 2 \sum_{i=0}^{N} \left(\frac{w_i^c}{s_i^2} \right)^2 \left(\left(\sigma_{y_i}^2 + \tilde{\sigma}_{\mu_y}^2 \right)^2 + 2 \left(\sigma_{y_i}^2 + \tilde{\sigma}_{\mu_y}^2 \right) (\mu_{y_i} - \tilde{\mu}_y)^2 \right) \tag{16}$$

It is true that (16) illustrates the uncertainty variance of the variance estimator. With this, we have knowledge of the confidence in the estimation of the variance. For the purposes of our work, this term is not immediately relevant, but we include it because of its equivalent derivation from the generalized χ^2 distribution and potential inclusion in future work.

2.3.3 Stochastic Unscented Transformation with Common Symmetric $N = 2$ Sigma Points

Recall from section 2.2.1, the two sigma points defined as $s_0 = +1$ and $s_1 = -1$ with weights as $w_0^a = w_1^a = w_0^c = w_1^c = \frac{1}{2}$. Inserting these values into the generalized mean and variance estimators yields

$$\tilde{\mu}_y = \frac{1}{2} \left(\mu_{y_0} + \mu_{y_1} \right) \tag{17}$$

$$\tilde{\sigma}_{\tilde{\mu}_y}^2 = \frac{1}{4} \left(\sigma_{y_0}^2 + \sigma_{y_1}^2 \right) \tag{18}$$

$$\tilde{\sigma}_y^2 = \frac{1}{2} \left(\sigma_{y_0}^2 + \sigma_{y_1}^2 + 2\tilde{\sigma}_{\tilde{\mu}_y}^2 + \left(\mu_{y_0} - \tilde{\mu}_y\right)^2 + \left(\mu_{y_1} - \tilde{\mu}_y\right)^2 \right) \tag{19}$$

$$= \frac{1}{2} \left(\sigma_{y_0}^2 + \sigma_{y_1}^2 + 2\tilde{\sigma}_{\tilde{\mu}_y}^2 + \frac{1}{2} \left(\mu_{y_0} - \mu_{y_1} \right)^2 \right) \tag{20}$$

Intuitively, we can now see the inherent contribution of incorporating the model uncertainty with the use of the stochastic unscented transform. By grouping the terms of (20), we realize the output variance uncertainty consists of 3 parts:

- The model/transform uncertainty: $\frac{1}{2} \left(\sigma_{y_0}^2 + \sigma_{y_1}^2 \right)$

[2] It is noted that (13) assumes that (10) is distributed independently of y_i, which is incongruent since (10) is dependent on y_i. As such, the variance terms of (13) and the resultant overall distribution may be considered as upper bounds.

- The transformed input distribution uncertainty (matching eq (9)): $\frac{1}{4}\left(\mu_{y_0} - \mu_{y_1}\right)^2$
- The uncertainty of the mean estimation: $\tilde{\sigma}^2_{\tilde{\mu}_y}$

Incorporating and accounting for all three of these terms derives the complete stochastic system characterization.

3. SUT CAR-MHF APPLICATION

The Constrained Admissible Region - Multiple Hypothesis Filter (CAR-MHF), originally developed by AFRL/RV, provides an all-in-one solution for three normally separate orbit determination functions as originally outlined in [28] with significant updates made from [29], [30], and [31]:

- **Observation Association (OA):** The assignment of observations to particular existing object tracks and identification of new objects
- **Orbit Determination (OD):** The update of an orbital object state vector with additional/new observation data
- **Initial Orbit Determination (IOD):** The creation and initialization of a new object state vector

With new probabilistic models becoming available for atmospheric density estimation, such as CHAMP-ML [6] , TIE-GCM ROPE [12], and HASDM-ML [10], a (new) uncertainty value is provided along with the (normal) atmospheric density estimate. To integrate the new atmospheric density uncertainties into CAR-MHF, we consider the application of the SUT to the underlying CAR-MHF unscented Kalman framework.

CAR-MHF utilizes a (deterministic) unscented Kalman filter (UKF) at the heart of its propagation step to update a prior state vector and uncertainty to a new time epoch. We call this a "deterministic" unscented propagation/transformation (UT) because the underlying propagator does not actually propagate covariance uncertainty, but only the state vector itself. For covariance propagation, an unscented approach is utilized to propagate two sigma-point perturbations about each state vector element[3] using the initial covariance uncertainty. Then, the deviations of the sigma-point propagations are utilized to compute an updated (final) c ovariance. In this w ay, t he i nitial c ovariance i s (deterministically) tracked through the dynamics of the propagation process to produce an updated final c ovariance. P rocess n oise is also added, which inflates t he c ovariance o ver t he p ropagation t ime i nterval t o a ccount f or u nknown o r unmodeled dynamics.

It should be noted that only the propagation step of CAR-MHF is modified to support the incorporation of atmospheric drag uncertainty. The other major components of CAR-MHF (Kalman state update, constrained admissible region (CAR) IOD, and joint-probabilistic data association (JPDA) observation association [32]) are left unchanged.

3.1 SUT Integration for Probabilistic Drag

Application of the SUT requires a "probabilistic" dynamics model so that the SUT can not only track the propagated uncertainty (with process noise), but also the (new) uncertainties associated with the underlying dynamics of the modeling itself. However, "deterministic" unscented propagation can itself be considered as a "probabilistic" dynamics model, because it (via its deterministic unscented approach) provides not only an updated state vector but a updated covariance uncertainty as well. With this, one possible application is to *bootstrap* the existing CAR-MHF (deterministic) unscented approach with the SUT, by using the existing CAR-MHF propagation as the underlying SUT probabilistic dynamics model.

To incorporate a new probabilistic atmospheric density model, we can incorporate the density with its uncertainty estimate as the SUT initial uncertainty. Using the density uncertainty, we can create two density sigma-points: density $+1\sigma$ and density -1σ. Given each sigma-point, one can run the CAR-MHF deterministic unscented propagation with the associated sigma-point density. With this, a resultant state vector and covariance is produced for each density sigma-point, and the SUT can be used to combine these into a single state-vector and convariance that accounts for the overall system (including density) uncertainty.

[3]CAR-MHF utilizes 6 state vector elements to track each object's Cartesian position and velocity along with 2 additional state vector elements for drag (C_dA/m) and SRP (C_rA/m) estimation. For these 8 (total) state vector elements, two sigma-points are propagated for each, resulting in 16 propagations per state.

Figure 2 illustrates the conceptual flow for incorporating the SUT into CAR-MHF to include the uncertainty effects conveyed by a probabilistic atmospheric density model. The two density sigma-points are shown in the diagram separated by the central dashed line, where each density sigma-point propagation is controlled by a $\pm\sigma$ designation. The same prior state v and covariance P is provided to both density-sigma point propagations. Since each density sigma-point utilizes 16 underlying deterministic sigma-point propagations each, 32 total propagational variants are computed. Finally, the outputs of each density sigma-point are combined via the SUT to produce the final aggregated SUT propagated output, v' and P'.

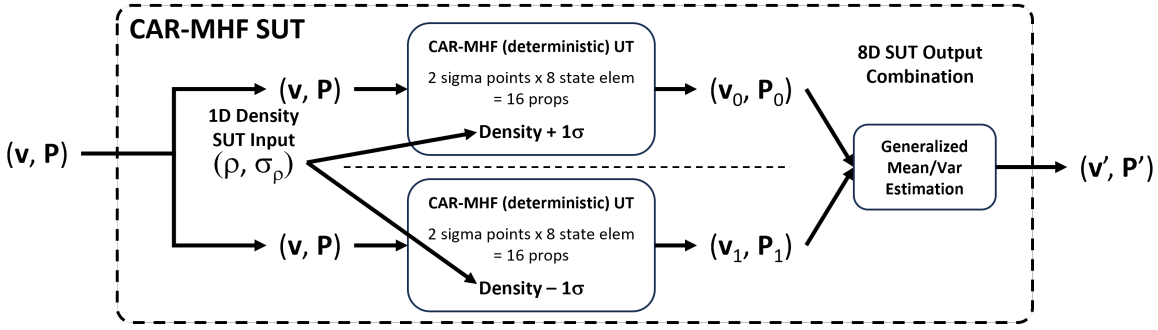

Fig. 2: CAR-MHF SUT incorporation for inclusion of probabilistic atmospheric density uncertainty [4]

When propagating the CAR-MHF (deterministic) UT, it is important to note that atmospheric density is re-evaluated/re-computed at each propagator integration variable time-step. For this, the resulting computation and density that is used for propagation is given as

$$\rho_i = \rho + s_i \sigma_\rho, \tag{21}$$

where ρ_i is the density applied for propagation, ρ is the calculated (mean) density, σ_ρ is the calculated density uncertainty standard deviation, and s_i is $+1$ or -1 depending on the chosen density sigma point. While ρ and σ_ρ (and also ρ_i) are recalculated at each integrator variable time step, s_i remains constant for a given propagation. With this way, each density sigma-point propagation remains statistically consistent in their assessed densities, i.e., one sigma-point consistently uses a higher density, while the other sigma-point consistently uses a lower density.

Propagation is conducted using Orekit numerical propagation [33], which has been integrated into CAR-MHF. Using (21), drag force acceleration, α_i is computed at each integrator variable time step as

$$\alpha_i = \frac{1}{2}\rho_i v^2 C_d \frac{A}{m}, \tag{22}$$

where v is the satellite atmospheric velocity, C_d is the coefficient of drag, A is the effective drag area, and m is the satellite mass.

According to SUT equations (10) and (15), the final SUT combination of the density sigma-point values is given as

$$\mathrm{v}' = \frac{1}{2}\left(\mathrm{v}_0 + \mathrm{v}_1\right) \tag{23}$$

$$\mathrm{P}_{\mathrm{v}'} = \frac{1}{4}\left(\mathrm{P}_0 + \mathrm{P}_1\right) \tag{24}$$

$$\mathrm{P}' = \frac{1}{2}\left(\mathrm{P}_0 + \mathrm{P}_1 + 2\mathrm{P}_{\mathrm{v}'} + \left(\mathrm{v}_0 - \mathrm{v}'\right)\left(\mathrm{v}_0 - \mathrm{v}'\right)^T + \left(\mathrm{v}_1 - \mathrm{v}'\right)\left(\mathrm{v}_1 - \mathrm{v}'\right)^T\right) \tag{25}$$

where v' is the mean state vector estimate, $\mathrm{P}_{\mathrm{v}'}$ is the uncertainty covariance associated with the mean v' estimate, and P' is the overall uncertainty covariance (inclusive of both the dynamics uncertainty and the atmospheric density uncertainty). As noted in [4], the inclusion of the mean estimate uncertainty, $\mathrm{P}_{\mathrm{v}'}$, is known to bias the resultant covariance, P'. To produce an unbiased covariance estimate, we do not include the contribution of $\mathrm{P}_{\mathrm{v}'}$, resulting in

$$\mathrm{P}' = \frac{1}{2}\left(\mathrm{P}_0 + \mathrm{P}_1 + \left(\mathrm{v}_0 - \mathrm{v}'\right)\left(\mathrm{v}_0 - \mathrm{v}'\right)^T + \left(\mathrm{v}_1 - \mathrm{v}'\right)\left(\mathrm{v}_1 - \mathrm{v}'\right)^T\right). \tag{26}$$

3.2 Computational Complexity

The primary advantage of the SUT bootstrapped implementation of the deterministic unscented propagation/transform is that the probabilistic influence of the atmospheric density model is inherently mapped directly into the density sigma-point covariance uncertainties. No consider parameters, augmented state vectors, or additional cross-correlations are necessary.

A disadvantage of this approach is that the total number of propagations increase by a factor equal to the number of probabilistic sigma-points. In this application for atmospheric density, two density sigma-points are utilized, so the total number of propagations increase by 2x (from 16 to 32) compared to the number of deterministic propagations.

If a consider parameter approach was used instead, only two additional propagations are necessary to account for the single augmented state. However, additional cross-correlations must be subsequently performed to consider the effects of the additional density state upon the position and velocity state elements.

3.3 Expected Results

As atmospheric density is directly proportional to the drag force acceleration (22), the density uncertainty is proportional to a linear increase in uncertainty over propagation time step intervals. In this way, density uncertainty acts as a form of inherent process noise. With this, we expect a (near) linear increase in uncertainty that will be most apparent during long inter-observation propagation intervals, such as LEO satellite intervals between ground-site access locations.

Since the uncertainty associated with atmospheric density is now properly being estimated, modeled, and aggregated, it is no longer necessary to account for this uncertainty using explicit process noise. Therefore, with this SUT approach, total process noise (meant to account for unknown dynamics) can be decreased as the process noise for atmospheric density is automatically being incorporated and accounted.

4. RESULTS

To illustrate the effects of probabilistic density estimation, simulated radar observation data was generated for a sun-synchronous satellite at 450km altitude using space-surveillance network (SSN) ground station locations. STK's high-precision orbital propatator (HPOP) was used to propagate the orbit for which NRL MSISE2000 was used to model atmospheric density and drag force using $C_dA/m = 0.044$. No measurement biases were simulated.

It should be noted that while STK HPOP was used to simulate the observation data, Orekit numerical propagation (and force modeling) is used within CAR-MHF. As a result, inherent differences between the two propagation methodologies and force modeling result in discrepancies.

To incorporate probabilistic density, a fixed uncertainty percentage was implemented alongside the NRL MSISE2000 density model. This was done to vary/control the amount of reported density uncertainty. It should be noted that this MSISE fixed uncertainty model can be replaced with CHAMP-ML, TIE-GCM ROPE, or HASDM-ML with no interface changes.

In processing the observations, CAR-MHF (without probabilistic density modeling) was tuned by adding spherical process noise until the McReynold's consistency test [34] passed using forward/backward fixed lag s moothing. For this data, 1e-5 m/s^2 was found to be sufficient.

Figures 3 and 4 show the resulting position uncertainty results over time. Figure 4 shows the results smoothed by forward/backward fixed lag smoothing, while Figure 3 shows the results with forward filtering on ly. In each figure, observation times are noted with dots. For each observation, pre-update and post-update uncertainties are plotted at each observation time. The "spikes" seen (primarily in the in-track results) are where the post-update uncertainty increases compared to the pre-update uncertainty after time intervals without observations. Here, the filter is applying a large correction after coasting without observations.

In the figures, note the particular coasting intervals without observations. These intervals are (initially) dominated by the inertial RIC rotation of the covariance uncertainty and (later) process noise. Since radar observations are employed here, the covariance uncertainty matrix is "pancake shaped" as the majority of innovation occurs along each sensor's line-of-sight.

With probabilistic density modeling, less process noise was needed for filtering tuning. With 50% density uncertainty,

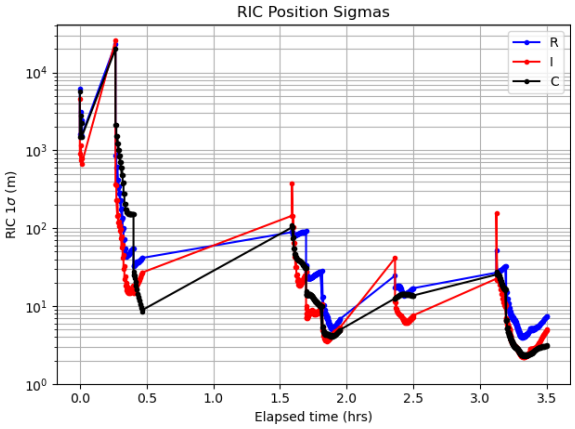

Fig. 3: Baseline Forward Position Uncertainty (without probabilistic density)

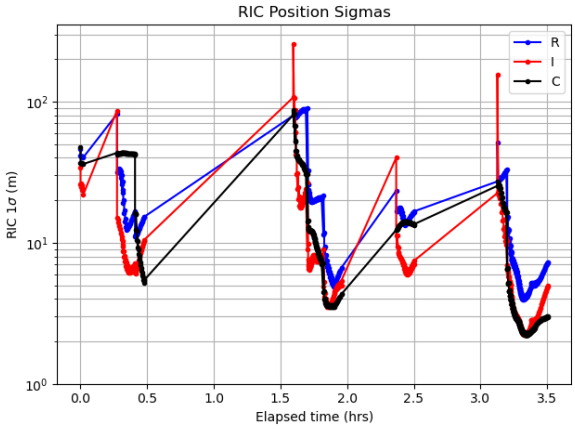

Fig. 4: Baseline Smoothed Position Uncertainty (without probabilistic density)

it was found that only 1e-5 m/s^2 process noise was needed (a factor of 10x less). This is as expected, because proper atmospheric density uncertainty modeling is eliminating the need for additional process noise.

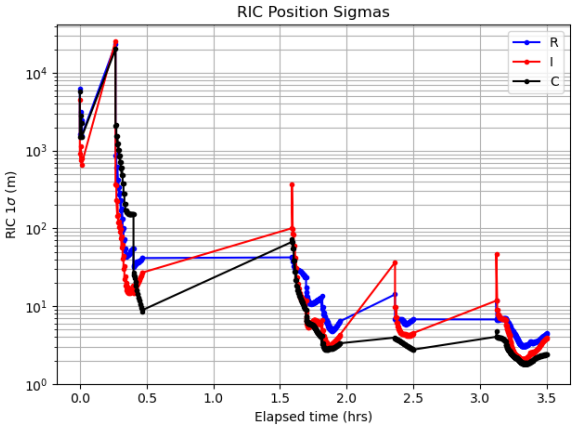

Fig. 5: Forward Position Uncertainty (with 50% probabilistic density)

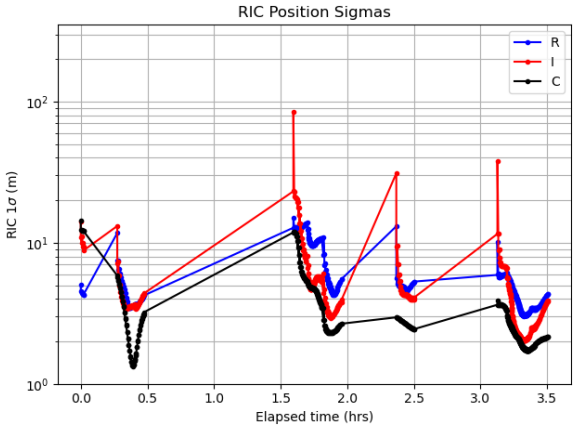

Fig. 6: Smoothed Position Uncertainty (with 50% probabilistic density)

Since the figure results are somewhat similar and difficult to compare visually, ratios were computed for probabilistic drag enabled and disabled. These ratios are shown in Figures 7 and 8 for the forward and smoothed cases respectively. Within these plots, lower ratios indicate lesser/improved accuracy. In Figure 7, we see uncertainty improvement over the baseline in all of the position components (R, I, and C), with the most improvement occurring, at first, in the radial component. This initial improvement is happening mostly due to the reduced process noise. Later, we observe the most improvement in the cross-track component (as, intuitively, atmospheric density uncertainty should not contribute to cross-track). We see some improvement in the radial, and the least improvement in in-track which are the directions where we expect the most uncertainty contribution from atmospheric density uncertainty.

A key takeaway here is that the SUT approach automatically computes and adds the uncertainty for the probabilistic uncertainties exposed to it. With this, one no longer needs to consider adding arbitrary process noise.

For the smoothed comparison shown in Figure 8, the results are less intuitive due to the forward-backward smoothing involved. However, an overall improvement is (again) noted in all of the components, with the cross-track component exhibiting the most overall improvement.

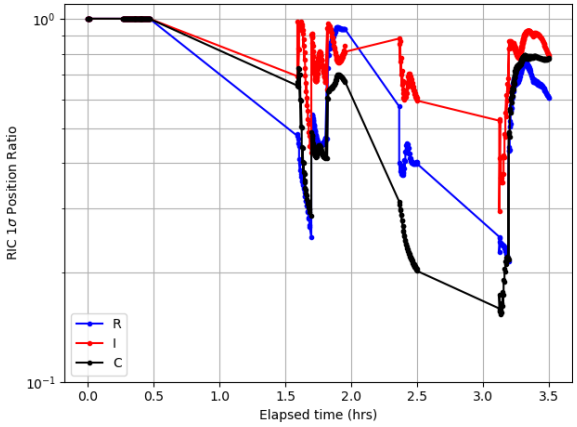

Fig. 7: Forward Position Uncertainty Ratio

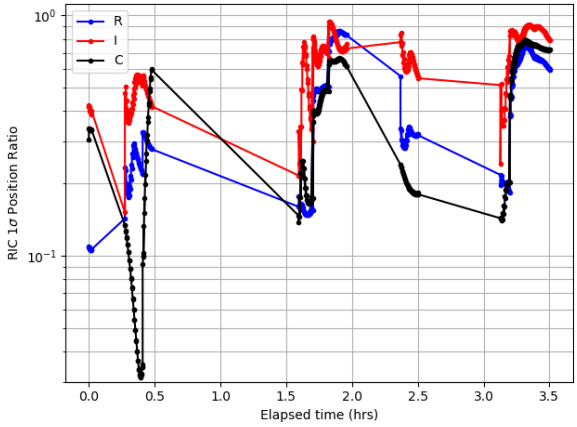

Fig. 8: Smoothed Position Uncertainty Ratio

5. CONCLUSIONS AND FUTURE WORK

A new unscented approach is presented that, in addition to accounting for and propagating apriori covariance, now also incorporates reported model uncertainties. This Stochastic Unscented Transform technique is theoretically derived and presented as a potential application for incorporating new probabilistic atmospheric density models into orbit determination. Using CAR-MHF, the approach showed that the additional atmospheric density uncertainty is accounted for and automatically applied similarly to process noise. With this uncertainty explicitly accounted for, the amount of necessary process noise was able to be decreased.

Additional probabilistic dynamic models, such as those for spacecraft attitude, spacecraft maneuvering, solar radiation pressure, and gravity can be considered and applied using this same technique, as the SUT technique is generic and can be used with any probabilistic model. Future work involves applying the technique to real satellite observation data using TIE-GCM ROPE and/or HASDM atmospheric density modeling.

REFERENCES

[1] R.J. III Licata. *Probabilistic Space Weather Modeling and Forecasting for the Challenge of Orbital Drag in Space Traffic Management*. Ph.D. dissertation, West Virginia University, 2022. URL https://researchrepository.wvu.edu/etd/11600.

[2] S.N. Paul, P.L. Sheridan, R.J. Licata, and P.M. Mehta. Stochastic modeling of physical drag coefficient – its impact on orbit prediction and space traffic management. *Advances in Space Research*, 72(4):922–939, 2023. ISSN 0273-1177. doi: https://doi.org/10.1016/j.asr.2023.06.006. URL https://www.sciencedirect.com/science/article/pii/S0273117723004362.

[3] S.N. Paul, R.J. Licata, and P.M. Mehta. Advanced ensemble modeling method for space object state prediction accounting for uncertainty in atmospheric density. *Advances in Space Research*, 71(6):2535–2549, 2023. ISSN 0273-1177. doi: https://doi.org/10.1016/j.asr.2022.12.056. URL https://www.sciencedirect.com/science/article/pii/S0273117722011723.

[4] R. Bhatia, G.J. Rivera Santos, J.D. Griesbach, and P.M. Mehta. A novel stochastic unscented transform for probabilistic drag modeling and conjunction assessment. In *Proceedings of the Advanced Maui Optical and Space Surveillance (AMOS) Technologies Conference*, September 2024.

[5] J.D. Daniell and P.M. Mehta. Probabilistic solar proxy forecasting with neural network ensembles. *Space Weather*, 21(9), 2023. doi: https://doi.org/10.1029/2023SW003675. URL https://agupubs.onlinelibrary.wiley.com/doi/abs/10.1029/2023SW003675.

[6] R.J. Licata and P.M. Mehta. Uncertainty quantification techniques for space weather modeling: Thermospheric density application. *Scientific Reports*, abs/2201.02067, 2022. URL https://arxiv.org/abs/2201.02067.

[7] M.F. Storz, B.R. Bowman, J.I. Branson, S.J. Casali, and W.K. Tobiska. High accuracy satellite drag model (HASDM). *Advances in Space Research*, 36(12):2497–2505, 2005. ISSN 0273-1177. doi: https://doi.org/10.1016/j.asr.2004.02.020. URL https://www.sciencedirect.com/science/article/pii/S0273117705002048.

[8] J.T. Emmert et al. NRLMSIS 2.0: A whole-atmosphere empirical model of temperature and neutral species densities. *Earth and Space Science*, 8(3), 2020. doi: https://doi.org/10.1029/2020EA001321. URL https://agupubs.onlinelibrary.wiley.com/doi/abs/10.1029/2020EA001321.

[9] W. Zhan, A. Doostan, E. Sutton, and T. Fang. Quantifying uncertainties in the quiet-time ionosphere-thermosphere using WAM-IPE. *Space Weather*, 22(2), 2024. doi: https://doi.org/10.1029/2023SW003665. URL https://agupubs.onlinelibrary.wiley.com/doi/abs/10.1029/2023SW003665.

[10] R.J. Licata, P.M. Mehta, W.K. Tobiska, and S. Huzurbazar. Machine-Learned HASDM Thermospheric Mass Density Model With Uncertainty Quantification. *Space Weather*, 20(4), 2022. doi: https://doi.org/10.1029/2021SW002915. URL https://agupubs.onlinelibrary.wiley.com/doi/abs/10.1029/2021SW002915.

[11] R.J. Licata, P.M. Mehta, D.R. Weimer, W.K. Tobiska, and J. Yoshii. MSIS-UQ: Calibrated and enhanced NRLMSIS 2.0 model with uncertainty quantification. *Space Weather*, 20(11), 2022. doi: https://doi.org/10.1029/2022SW003267. URL https://agupubs.onlinelibrary.wiley.com/doi/abs/10.1029/2022SW003267.

[12] R.J. Licata and P.M. Mehta. Reduced order probabilistic emulation for physics-based thermosphere models. *Space Weather*, 21(5):1542–7390, May 2023. doi: 10.1029/2022sw003345. URL http://dx.doi.org/10.1029/2022SW003345.

[13] S.J. Julier and J.K. Uhlmann. Unscented filtering and nonlinear estimation. *Proceedings of the IEEE*, 92(3): 401–422, 2004. doi: 10.1109/JPROC.2003.823141.

[14] H.W. Sorenson. *Kalman Filtering: Theory and Application*. New York:IEEE Press, 1985. ISBN 0879421916. URL https://api.semanticscholar.org/CorpusID:117189881.

[15] S.J. Julier and J.K. Uhlmann. New extension of the kalman filter to nonlinear systems. In *Proceedings of the SPIE*, volume 3068, pages 182–193, 1997. URL https://api.semanticscholar.org/CorpusID:7937456.

[16] J. Stauch and M. Jah. Unscented schmidt–kalman filter algorithm. *Guidance, Control, and Dynamics*, 38(1): 117–123, 2015. doi: 10.2514/1.G000467. URL https://doi.org/10.2514/1.G000467.

[17] A. Manarvi and T. Henderson. Application of kalman filters in orbit determination: A literature review. In *6th International Conference on Astrodynamics Tools and Techniques (ICATT)*, 2016. URL https://indico.esa.int/event/111/contributions/392/attachments/555/600/Application_of_Kalman_Filters_in_Orbit_Determination_A_Literature_Survey.pdf.

[18] R. Armellin, P. Di Lizia, and R. Zanetti. Dealing with uncertainties in angles-only initial orbit determination. *Celestial Mechanics and Dynamical Astronomy*, 125(4):435–450, August 2016. doi: 10.1007/s10569-016-9694-z. URL https://doi.org/10.1007/s10569-016-9694-z.

[19] T. Kelecy, M. Shoemaker, and M. Jah. Application of the constrained admissible region multiple hypothesis filter to initial orbit determination of a break-up. In *6th European Conference on Space Debris*, August 2013. URL https://ui.adsabs.harvard.edu/abs/2013ESASP.723E..65K.

[20] N. Stacey and S. D'Amico. Analytical process noise covariance modeling for absolute and relative orbits. *Acta Astronautica*, 194:34–47, 2022. ISSN 0094-5765. doi: https://doi.org/10.1016/j.actaastro.2022.01.020. URL https://www.sciencedirect.com/science/article/pii/S0094576522000297.

[21] M. Schubert, C. Kebschull, and S. Horstmann. Analysis of different process noise models in typical orbit determination scenarios. In *8th European Conference on Space Debris*, April 2021.

[22] F.H. Schlee, C.J. Standish, and N.F. Toda. Divergence in the Kalman filter. *AIAA Journal*, 5(6):1114–1120, 1967. doi: 10.2514/3.4146. URL https://doi.org/10.2514/3.4146.

[23] D. McKnight, R. Bhatia, E. Dale, C. Gates, O. Marshall, A. Marsh, and M. Patel. Analytic space domain awareness. In *Proceedings of the Advanced Maui Optical and Space Surveillance (AMOS) Technologies Conference*, September 2023.

[24] R. Bhatia and D. McKnight. Assessment of evolving conjunction risk for small satellite missions. In *Small Satellite Conference*, 2023.

[25] D. Ebeigbe et al. A generalized unscented transformation for probability distributions. 2021. URL https://arxiv.org/abs/2104.01958.

[26] S.J. Julier and J.K. Uhlmann. New extension of the kalman filter to nonlinear systems. In *Proceedings of the SPIE*, volume 3068, pages 182–193, 1997. URL https://api.semanticscholar.org/CorpusID:7937456.

[27] E.A. Wan and R. Van Der Merwe. The unscented kalman filter for nonlinear estimation. In *Proceedings of the IEEE 2000 Adaptive Systems for Signal Processing, Communications, and Control Symposium (Cat. No.00EX373)*, pages 153–158, 2000. doi: 10.1109/ASSPCC.2000.882463.

[28] K. DeMars and M. Jah. Passive multi-target tracking with application to orbit determination for geosynchronous objects. *AAS Paper 09-108, 19th AAS/AIAA Space Flight Mechanics Meeting*, 2009.

[29] T. Kelecy and M. Jah. Analysis of high area-to-mass ratio (HAMR) GEO space object orbit determination and prediction performance: Initial strategies to recover and predict HAMR GEO trajectories with no a priori information. *Acta Astronautica*, 69(7):551–558, 2011. ISSN 0094-5765. doi: https://doi.org/10.1016/j.actaastro.2011.04.019.

[30] J. Stauch, M. Jah, J. Baldwin, T. Kelecy, and K. Hill. Mutual application of joint probabilistic data association, filtering, and smoothing techniques for robust multiple space object tracking. *AIAA/AAS Astrodynamics Specialist Conference 2014*, August 2014. doi: 10.2514/6.2014-4365.

[31] I.I. Hussein, C.W.T. Roscoe, M. Mercurio, M.P. Wilkins, and P.W. Schumacher Jr. Probabilistic admissible region for multihypothesis filter initialization. *American Institute of Aeronautics and Astronautics (AIAA)*, 41(3), 2018. ISSN 1533-3884. doi: https://doi.org/10.2514/1.G002788.

[32] T. Fortmann, Y. Bar-Shalom, and M. Scheffe. Sonar tracking of multiple targets using joint probabilistic data association. *IEEE Journal of Oceanic Engineering*, 8(3):173–184, 1983. doi: 10.1109/JOE.1983.1145560.

[33] Orekit space dynamics library, 2024. URL https://www.orekit.org.

[34] D.A. Vallado, T.S. Kelso, V. Agapov, and I. Molotov. Orbit determination issues and results to incorporate optical measurements in conjunction operations. In *Proceedings of the 5th European Conference on Space Debris*, ESA SP-672, Darmstadt, Germany, July 2009.